

Lindblad theory of dynamical decoherence of quantum-dot excitons, with applications to phonon spectroscopy and adiabatic rapid passage

P. R. Eastham,¹ A. O. Spracklen,² and J. Keeling²

¹*School of Physics, Trinity College, Dublin 2, Ireland.*

²*SUPA, School of Physics and Astronomy, University of St. Andrews, KY16 9SS, U.K.*

We discuss the application of the Bloch-Redfield-Wangsness theory to the effects of acoustic phonons in coherent control experiments with quantum-dot excitons. This approach yields a positivity preserving Markovian density matrix equation that captures the same essential physics as the form recently applied to Rabi oscillation experiments [A. J. Ramsay *et al.* Phys. Rev. Lett. 104, 017402 (2010)]. At sufficiently low temperature, it gives results equivalent to those of non-Markovian approaches [S. Lüker *et al.* Phys. Rev. B 85, 121302 (2012)], but is significantly simpler to simulate. Using this approach we discuss a number of applications including optimization of adiabatic rapid passage and phonon spectroscopy.

PACS numbers: 78.67.Hc, 03.65.Yz, 42.50.Hz, 71.38.-k

I. INTRODUCTION

Controlled manipulation of coherent quantum systems is a crucial requirement for quantum information technologies, can be exploited in ultrafast switches, and may allow the exploration of exotic regimes of quantum dynamics. An important example among solid-state systems is that of excitons in quantum dots,¹ which provide discrete atomic-like transitions that can be manipulated using optical pulses. These transitions have been demonstrated experimentally to correspond to two-level systems, for which resonant optical excitation induces Rabi oscillations.^{2,3} Thus under pulsed excitation the number of excitons created oscillates with the pulse area: a pulse of the correct duration and intensity creates exactly one exciton in the quantum dot, while other pulses create superpositions of one- and no- exciton states. Frequency-swept laser pulses have also been used to create single excitons in quantum dots, implementing the protocol of adiabatic rapid passage (ARP), and allowing state manipulation in a way which is robust against fluctuations in the coupling strengths and transition energies of the dots.⁴⁻⁷

A theoretical description of such coherent control experiments must capture both the dynamics of the driven quantum dot, and the scattering and decoherence introduced by the interaction between the dot and its environment. In particular, the coupling to acoustic phonons leads to dephasing of the Rabi oscillations⁸ and limits the inversion in ARP.^{4,5,9,10} (Optic phonons could play a role in ARP with very intense, very short pulses,¹¹ where the energy scales are comparable to the optic phonon energies, but we do not consider this regime here.) The standard theoretical approach¹² involves second-order perturbation theory in the phonon coupling, leading to an equation of motion for the reduced density operator of the dot. This equation involves an integral over all previous states of the dot, capturing the memory effects due to the finite bandwidth and response time of the environment.

The most popular approach to treating this type of non-Markovian equation of motion is a form of Markov approximation which reduces the equation to a time-local equation, with the effects of the phonons appearing as a constant Lindblad form describing dephasing. Such an equation would be valid under the assumption that the response time of the environment is the shortest timescale in the problem. This approximation, however, is generally incorrect for quantum dot excitons.^{13,14} It predicts that the environment induces transitions independently of the state of the dot, in contradiction to experiments in which the driving field changes the dephasing. Such dynamical excitation-dependent dephasing has, however, been successfully described by more sophisticated approaches. These include numerical solutions of the full integral equation,^{9,10,13,15} including all the memory effects of the environment, as well as time-local approximations^{8,14-17} to this equation, allowing for some of the memory effects neglected in the simplest form of Born-Markov approximation. This same point — that it is important to calculate the decay rates arising from system-bath coupling making use of the actual system Hamiltonian — is also crucial in describing the correct equilibrium state of strongly coupled systems, as discussed in Ref. 18.

In this paper, we discuss the application of the Bloch-Redfield-Wangsness^{19,20} (BRW) theory, widely used to describe nuclear spin relaxation, to coherent control experiments on excitons in quantum dots. It is similar to the simplest Born-Markov approximation, but allows the timescale set by the inverse level spacing of the Hamiltonian to be smaller than the response time of the environment. We use this theory to derive a generalized Lindblad form for the phonon-induced damping, in which the transition operators connect the time-dependent eigenstates of the dot, with the expected perturbative transition rates [Eq. (7)]. This differs from the simplest Lindblad form mentioned above, which is often applied to quantum dots, in which the transition operators do not necessarily connect eigenstates. Furthermore, in con-

trast to the forms obtained by some other time-local approximations,^{14,16} it guarantees the positivity of the density operator, and so can be used across a wider variety of pulse shapes and temperatures. We focus on the application to determining the effects of phonons for adiabatic rapid passage in quantum dots, and show that the results are similar to those recently obtained by numerical solutions of the full integral equation.^{9,10} Thus Eq. (7) provides a simple picture of the effects of dephasing and a lightweight computational approach for modeling dephasing in quantum dots. As a further application of this theory, we use it to demonstrate the feasibility of generalizing the ARP experiments to measure phonon spectra and distribution functions, implementing a type of multi-dimensional spectroscopy for excitons.

The remainder of this paper is structured as follows. In Sec. II, we outline the derivation of the equation of motion for a driven quantum dot interacting with acoustic phonons. In Sec. III, we present the predictions of this equation for the inversion (exciton occupation) obtained in ARP, discuss how this process may be optimized in the presence of phonon-induced dephasing, and explain why the dephasing can in some circumstances improve the final inversion. In Sec. IV we use it to propose and analyze two forms of spectroscopy, in which the final inversion reached is used to measure the density-of-states of the phonons. In Sec. V, we discuss further the relationship between the positivity-preserving Lindblad form [Eq. (7)] obtained here and the generally positivity-violating precursor to this form [Eq. (4)], which is sometimes used directly.^{14,16} We present numerical results showing the failure of this latter approximation in the case of ARP pulses. In Sec. VI we summarize our conclusions. Finally, Appendices A and B provide details of the derivations of Eqs. (7) and (13) respectively.

II. EQUATIONS OF MOTION

In this section, we present the derivation of the secularized (Lindblad) form of the density matrix equations of motion. Our approach initially follows the same steps as in Refs. 14 and 16. However, in order to produce an approach that preserves positivity of the density matrix throughout the range of validity of perturbation theory, we must additionally secularize the resulting equations.^{21,22} For completeness, we include in this paper also the steps which follow Refs. 14 and 16. In this section we outline the main steps of the derivation, and present further details in appendix A.

We consider a single quantum dot, driven close to one of its discrete transition frequencies by a laser pulse with a time-dependent amplitude and frequency. For simplicity we assume that the excitation is circularly polarized, so that only one of the exciton spin states is relevant and we may neglect the formation of biexcitons. Thus we model the dot as a two-level system, which may be in the ground state, $|0\rangle$, or the one-exciton state, $|X\rangle$. The

Hamiltonian may be expressed, using pseudospin-1/2 operators \mathbf{s} , as ($\hbar = 1$)

$$H_{\text{dot}} = \Delta(t)s_z - \Omega(t)s_x, \quad (1)$$

in the rotating-wave approximation, and in a frame rotating at the instantaneous driving frequency $\omega(t)$. Here $\Delta(t) = E_0 - \omega(t)$ is the detuning between the transition energy E_0 and the instantaneous driving frequency. $\Omega(t)$ is the time-dependent Rabi frequency, corresponding to the amplitude of the driving pulse. $\mathbf{s} = \sigma/2$, where the Pauli operator $\sigma_z = |X\rangle\langle X| - |0\rangle\langle 0|$ describes the occupation of the exciton state, while $\sigma_x = |X\rangle\langle 0| + |0\rangle\langle X| = s_+ + s_-$ describes the electric dipole moment of the transition. We refer to $s_z = \sigma_z/2$ as the inversion.

We focus on the effects of acoustic phonons, which are the dominant dephasing mechanism in recent Rabi flopping^{14,16} and ARP experiments.^{4,5,9,10} They couple to the dot via the deformation potential coupling,

$$H_c = s_z \sum_q (g_q b_q + g_q^* b_q^\dagger), \quad (2)$$

where q labels the phonon wavevectors, b_q (b_q^\dagger) is a phonon annihilation (creation) operator, and g_q is the coupling constant. The phonon effects are controlled by the phonon spectral density, $J(\omega) = \sum_q |g_q|^2 \delta(\omega - \omega_q)$. We take the model¹⁴ for a GaAs/InGaAs quantum dot:

$$J(\omega) = \frac{\hbar A}{\pi k_B} \omega^3 e^{-\omega^2/2\omega_c^2}, \quad (3)$$

with $A = 11.2 \text{ fs K}^{-1}$, $\hbar\omega_c = 1.4 \text{ meV}$. In Eq. (3) the low-frequency behavior $J(\omega) \propto \omega^3$ arises from the coupling and density-of-states for acoustic phonons, while the high-frequency cut-off at ω_c arises from the size of the dot; confined excitons do not couple effectively to phonons of wavelengths smaller than the confinement.

In the limit that $\Delta(t), \Omega(t)$ vary slowly with time, we may treat them effectively as constant and use the approach discussed in Refs. 14 and 16, so that the effect of the acoustic phonons can be found by transforming to the interaction picture, and using the Born-Markov approximation there. This requires that the interaction-picture density operator is approximately constant over the correlation time of the phonon bath ($\sim 1/\omega_c$), so that $\tilde{\rho}(t') \simeq \tilde{\rho}(t)$ on the right-hand side of Eq. (A4). Equivalently, this means that the bath density of states should be flat over the effective linewidth of the system, as illustrated in Fig. 1. Such an approximation is valid as long as neither the decay rate nor sweep rates ($\dot{\Delta}/\Delta, \dot{\Omega}/\Omega$) are too high, as both contribute to the effective linewidth. Note that applying the Born-Markov approximation directly in the Schrödinger picture requires additionally that the density of states is flat on the scale of the range of position of the line, i.e., the energy scale of the Hamiltonian, and this is not the case here.

It is convenient to introduce rotated spin operators $\mathbf{r} = R\mathbf{s}$, with R a rotation by angle $\tan^{-1} \Omega/\Delta$ around

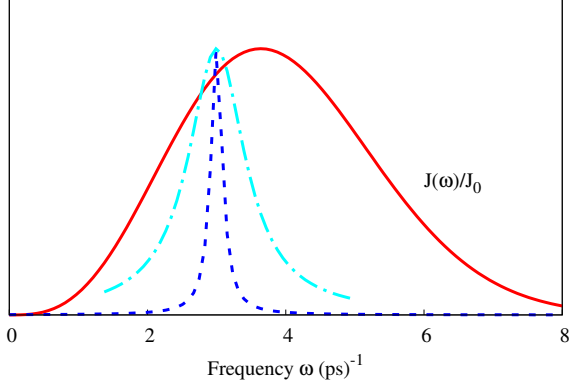


FIG. 1. (color online). Illustration of timescales required for validity of (time-dependent) Markov approximation, shown in the frequency domain. Solid red line shows the frequency dependent decay rate, illustrated by the phonon spectral function $J(\omega)$. At low temperatures and slow driving (dashed line), the linewidth is sufficiently small that the decay rate does not vary significantly across the linewidth (bath correlation time is short compared to decay time). At higher temperatures, or faster driving, the linewidth grows (dot-dashed line) so that the decay rate does vary (decay time or sweep time become comparable to bath correlation time). The line-shapes illustrated are Lorentzians corresponding to transition rates $T_1^{-1} = 0.2$ and 1.0 ps^{-1} , which may be compared with Fig. 2.

the y-axis, so that the instantaneous system Hamiltonian becomes $H_{\text{dot}} = \Lambda r_z$ where $\Lambda = \sqrt{\Omega^2 + \Delta^2}$. For the acoustic phonon coupling considered here, this yields (see Appendix A for further details):

$$\dot{\rho} = -PQ\tilde{\rho} + Q\tilde{\rho}P + P\tilde{\rho}Q^\dagger - \tilde{\rho}Q^\dagger P \quad (4)$$

where P, Q are time-dependent operators of the form:

$$P(t) = \frac{\Delta}{\Lambda} r_z + \frac{\Omega}{2\Lambda} (r_+ e^{i\Lambda t} + r_- e^{-i\Lambda t}), \quad (5)$$

$$Q(t) = \int d\nu J(\nu) \int_{t'}^t dt' P(t') \times \left[(n_\nu + 1) e^{-i\nu(t-t')} + n_\nu e^{i\nu(t-t')} \right], \quad (6)$$

and n_ν is the phonon occupation function at frequency ν . After undoing the transformation to the interaction picture, this gives the density matrix equation form corresponding to the results in Ref. 16.

This equation is not of Lindblad form, and consequently it can lead to density matrix evolution which violates positivity. For the relatively short pulses in Ref. 14 and 16, one may readily check that this is not a problem. However, for our application to ARP pulses, positivity violation can occur at late times under conditions where the perturbative approximations required for Born-Markov remain valid; this is discussed further in Sec. V

This issue of positivity violation was discussed extensively in, e.g., Ref. 21, where it was shown that there exists more than one form of Markovian density matrix equation which faithfully represents the infinitesimal increment of the full density matrix evolution in the Markovian (perturbative) limit. However, although these different forms are equivalent regarding infinitesimal timesteps, those equations that are not of Lindblad form do not conserve positivity. A Lindblad form can nonetheless be derived by averaging so as to remove the rapidly oscillating terms in Eq. (4) — such a procedure, known as secularization, yields a Lindblad form that in the perturbative limit is equally valid to Eq. (4). Further details are presented in the appendix; the result is:

$$\begin{aligned} \dot{\rho} = & -[\gamma_a(\Omega, \Delta)/2](r_- r_+ \rho + \rho r_- r_+ - 2r_+ \rho r_-) \\ & -[\gamma_e(\Omega, \Delta)/2](r_+ r_- \rho + \rho r_+ r_- - 2r_- \rho r_+) \\ & - i[r_z, \rho](\Lambda + \Delta E(\Omega, \Delta)), \end{aligned} \quad (7)$$

where we have made explicit the time dependence of the decay rates due to the dependence on the slow variation of the parameters $\Omega(t), \Delta(t)$. This is a time-dependent generalization of the standard form¹⁹ obtained from the secularized Born-Markov approximation in the interaction picture, as used in some related contexts.^{23,24} In addition to now preserving positivity, it makes explicit the origin and nature of decay terms; the damping appears as a Lindblad form describing transitions between the instantaneous dressed states, with the phonon absorption and emission rates

$$\gamma_a = 2 \left(\frac{\Omega}{2\Lambda} \right)^2 \pi J(\Lambda) n(\Lambda) \quad (8)$$

$$\gamma_e = 2 \left(\frac{\Omega}{2\Lambda} \right)^2 \pi J(\Lambda) [n(\Lambda) + 1]. \quad (9)$$

These rates are shown in Fig. 2 for the spectral function Eq. (3). In addition, Eq. (7) includes a phonon Lamb shift (Fig. 3): the energy splitting of the dressed states is now $\Lambda + \Delta E$ with

$$\Delta E = - \left(\frac{\Omega}{2\Lambda} \right)^2 2\Lambda \int \frac{J(\nu) \coth(\nu/2kT)}{\nu^2 - \Lambda^2} d\nu. \quad (10)$$

Figure 2 may be used to establish the validity of Eq. (7), by comparing the decay rates with the extent of their frequency dependence. We see that at the highest temperatures shown the peak damping rates, and therefore the linewidths, can become a significant fraction of the width of the spectral function, as illustrated in Fig. 1. In this regime the Markovian approximation that $\tilde{\rho}(t)$ varies slowly on the timescale $1/\omega_c$ breaks down, and a quantitative analysis requires the solution of a non-local equation.^{9,10} However, as can be seen from the linewidths in Fig. 1, we expect qualitatively reasonable results over much of the parameter regimes shown, and the approximations should be quantitatively accurate in the low temperature regime, below 20K, typical of most coherent

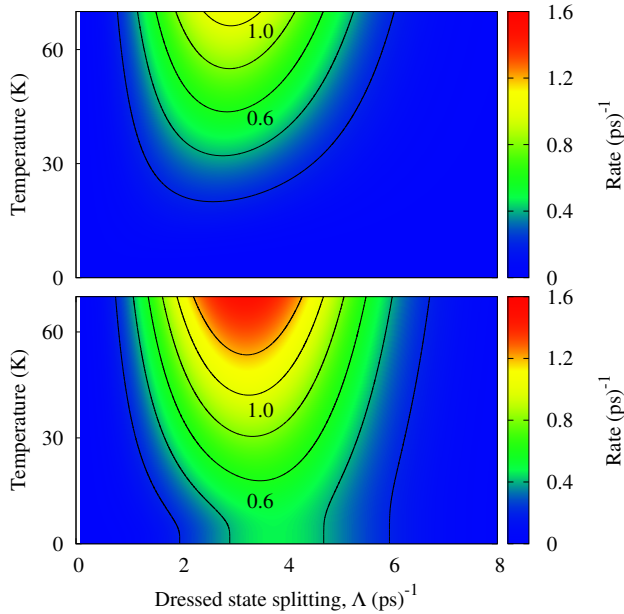


FIG. 2. (color online). Phonon absorption (top) and emission (bottom) rates, Eqs. (8) and (9), divided by the squared ratio of Rabi splitting to dressed-state energy splitting, Ω^2/Λ^2 , as a function of the dressed-state energy splitting $\Lambda = \sqrt{\Omega^2 + \Delta^2}$; for resonant driving $\Delta = 0$ and the scaling is one.

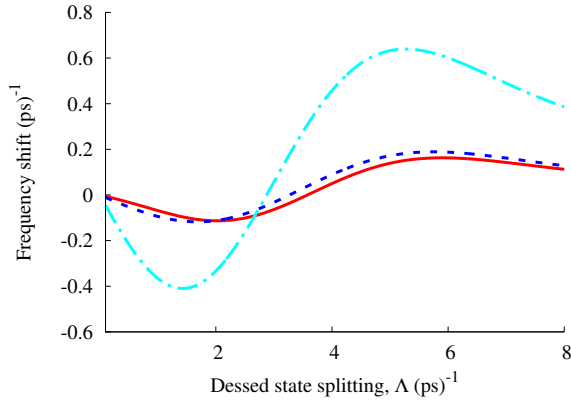


FIG. 3. (color online). Phonon-induced change in the dressed-state splitting ΔE [Eq. (10)] divided by the squared ratio of Rabi splitting to dressed-state energy splitting, i.e., $\Delta E/(\Omega^2/\Lambda^2)$, as a function of the dressed-state energy splitting Λ . Curves are temperatures 1K (solid), 10K (dashed), 50K (dot-dashed).

control experiments. We note that the Markov approximation amounts to approximating the spectral function with its constant value at the dressed frequency Λ . At high temperatures the damping at any one splitting will sample a finite range of the spectral function, so that we expect a weaker dependence of the effective linewidth on the energy splittings than indicated here, as well as non-Lorentzian emission lines. Similarly, we expect the

Markov approximation to overestimate the Lamb shift and its frequency dependence at high temperatures.

As well as becoming invalid at high temperatures, where the effective linewidth becomes large due to scattering, the approximations used above also fail if the time dependence of the parameters $\Delta(t), \Omega(t)$ becomes too strong. This is due to the finite bandwidth $1/\tau_{\text{chirp}} \sim \dot{\Delta}/\Delta$ arising from the time dependence of the parameters. Alternatively one may understand this as arising from the fact that for small enough τ_{chirp} , the bath correlation time no longer is the shortest timescale in the problem.

III. INVERSION IN ARP

The above results apply in general to any time-dependent pulse sequence. We can in particular consider pulses corresponding to adiabatic rapid passage, in which the detuning $\Delta(t)$ is swept smoothly through zero with the intention of creating a one-exciton state. Under such a pulse there is an avoided crossing between the zero- and one- exciton states of Eq. (1) generated by the driving field, and we aim to adiabatically follow this energy level, evolving from the initial ground state to the one exciton state. Acoustic phonon effects in this process have already been explicitly considered in Ref. 9 and 10, for fixed-bandwidth pulses of the form

$$\begin{aligned} \Delta(t) &= -\frac{at}{2(a^2 + \tau_0^4)}, \\ \Omega(t) &= \frac{\Theta_0}{\sqrt{2\pi\sqrt{a^2 + \tau_0^4}}} \exp\left(-\frac{t^2\tau_0^2}{2(a^2 + \tau_0^4)}\right), \end{aligned} \quad (11)$$

where Θ_0 is the area of the bandwidth-limited pulse before the chirp is applied, and a is the spectral chirp.²⁵ The results obtained from Eq. (4) for this form of pulse, plotted on a similar scale to those in Fig. 2 of Ref. 9, are shown in Fig. 4. As expected from the discussion above, the results are very similar at low temperatures and slow sweep rates, where the conditions for the Born-Markov approximation are well satisfied.

As discussed in Ref. 9, the asymmetry about the line $a = 0$ at low temperatures arises because absorption processes can be neglected $\gamma_a \ll \gamma_e$ for $T \ll \omega_c$, and as is clear from Eq. (7), emission can only occur when the dot is in the higher-energy dressed state. For $a < 0$ the ARP protocol attempts to follow this higher energy dressed state, so that the process is susceptible to phonon emission, whereas for $a > 0$ it is not. The simplicity of Eq. (7) allows one to further see that for the range plotted, the values of $\Lambda(t=0) = \Omega(t=0)$ lie below the peak of scattering rates (Fig. 2), hence the decrease of inversion with increasing pulse area visible within Fig. 4. For larger pulse areas, the central value of Λ can exceed this peak (at $\Theta_0 \approx 6\pi$ for $a = 0$), and inversion then increases with pulse area.

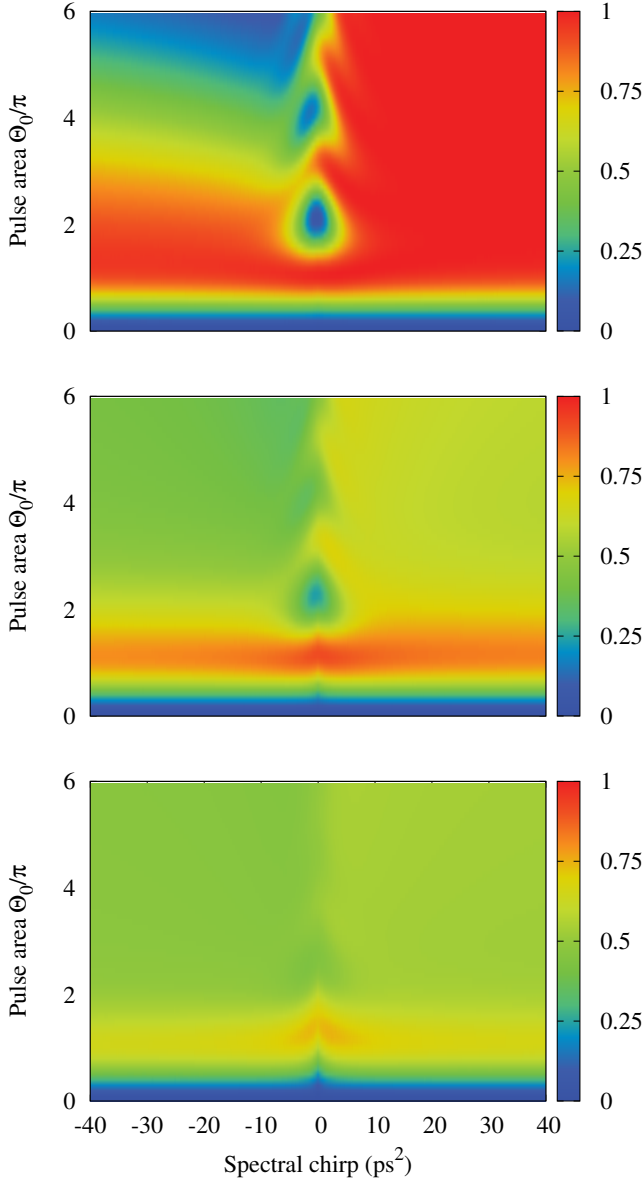


FIG. 4. (color online). Final exciton occupation probability following an ARP pulse of the form given in Eq. (11), calculated using the time-dependent Lindblad form given in Eq. (7). Calculated using $\tau_0 = 2$ ps, at temperatures 1K, 20K and 50K (top to bottom) for direct comparison with Fig. 2 of Ref. 9. For low temperatures, and slow sweeps, the results are very similar; for larger temperatures and higher chirp rates the limited Markov approximation used in deriving Eq. (7) becomes invalid.

A. Optimization of ARP

The relatively lightweight effort of simulating Eq. (7) allows one to rapidly investigate the effects of other potential pulse shapes and ARP protocols beyond that in Eq. (11). In the absence of decay, the question of how final excited state population can be optimized for a given pulse area has been extensively studied by Guérin

*et al.*²⁶. By considering the leading order non-adiabatic effects, they showed that these were minimized in the case where $\Lambda(t)$ was independent of time. This implies that in the limit of large pulse areas (deep in the adiabatic regime), maximum excitation should be reached when the chirp rate is adjusted to match this condition.

The time dependence of Δ, Ω given in Eq. (11) cannot achieve a time independent Λ . Instead, other pulse shapes need to be considered, such as:

$$\Delta(t) = -\Delta_0 \tanh\left(\frac{t}{\tau}\right), \quad \Omega(t) = \Omega_0 \operatorname{sech}\left(\frac{t}{\tau}\right), \quad (12)$$

which has a pulse area Θ when $\Omega_0 = \Theta/\tau$. As discussed by Guérin *et al.*²⁶, the optimum condition $\Omega_0 = \Delta_0$ arises from the convergence of lines originating from the maxima of the Rabi oscillations. This is shown in the inset of Fig. 5. However, although such pulses are optimal in the isolated case, the differences in excitation near this line are exponentially small, and entirely dwarfed by the effects of phonon induced dephasing. In the presence of dephasing, not only are the sharp, exponentially small features washed out, but the optimum chirp rate α moves to significantly larger values, due to the reduction of the dephasing rate with at sufficiently large Λ .

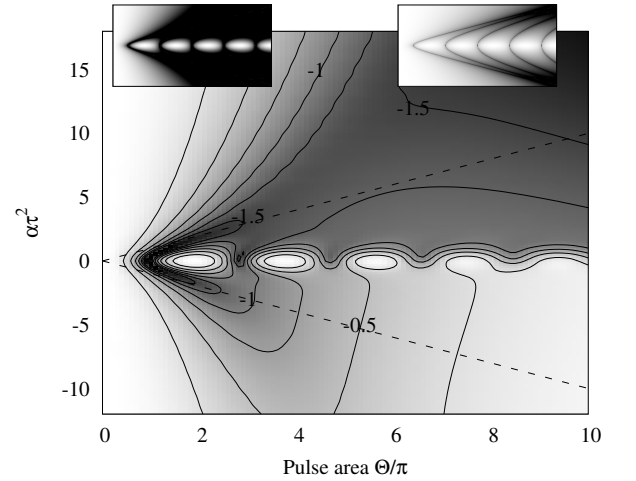


FIG. 5. Final exciton occupation probability for the sech pulse [Eq. (12)] with $\Omega_0 = \Theta/\tau, \Delta_0 = \alpha\tau$ for $\tau = 6$ ps at a temperature 4 K. The gray scale and contour labels show $\log_{10}(1 - P)$ where P is the final occupation probability. Insets show the case without phonon induced dephasing, as in Ref. 26, on the same gray scale (from -2 to 0, left inset), and on a gray scale with a larger range (from -10 to 0, right inset). Main panel shows the effects of dynamical dephasing on the same pulse shape. Dashed line indicates the condition $\Omega_0 = \Delta_0$ which gives the optimal transfer in the absence of dephasing.

B. Thermalization enhanced inversion

The discussion of the effects of acoustic phonons so far has been in terms of their reducing the final state inversion as compared to near-perfect inversion achieved deep in the adiabatic regime. There exists however a significant range of experimental conditions for which coupling to phonons can instead enhance the final state inversion. This effect has recently been discussed by Reiter *et al.*¹⁰ in the context of compensating for detuning of quantum dots. Even in the absence of detuning, coupling to phonons can enhance the final state inversion.

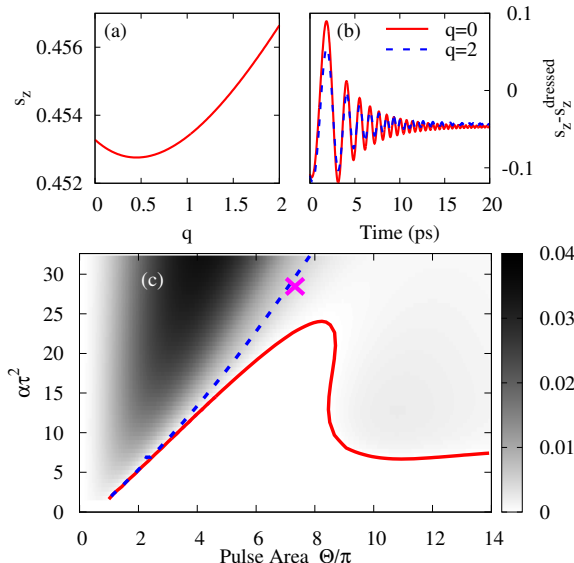


FIG. 6. (color online). Dependence of inversion on strength of phonon coupling in ARP. Panel (a) indicates how for a specific value of α, Ω_0 , there is a non-monotonic dependence of inversion upon phonon coupling. Panel (b) indicates the time evolution of s_z at two values of q , relative to its ideal value for adiabatically following the dressed states. Panel (c) maps where non-monotonic dependence on q arises. This is determined by two quantities: the grayscale indicates the value of $\text{Max}_{0 < q < 2}(ds_z/dq)$, and the solid red line is the boundary where this is zero. The blue dashed line indicates where $ds_z/dq|_{q=0} = 0$. Between these lines, non-monotonic dependence as seen in panel (a) occurs. The magenta cross indicates the conditions used for panels (a) and (b). $T = 4\text{K}$, $\tau = 5.68\text{ps}$

Figure 6 illustrates this potential enhancement by showing how the final inversion is affected if the decay rates are rescaled by a factor q , i.e. $J(\omega) \rightarrow qJ(\omega)$, considering a pulse shape:

$$\Omega = \Omega_0 \text{sech}\left(\frac{t}{\tau}\right), \quad \Delta = -\alpha t. \quad (13)$$

For a wide range of parameters Θ, α the dependence on q is non-monotonic: small coupling to phonons decreases the inversion, but further increase in coupling then increases final inversion. This non-monotonic behavior

[shown in Fig. 6(a)] exists throughout the region between the solid and dashed lines in Fig. 6(c). For large chirp rates and weak pulses, the inversion without coupling to phonons is already poor, and coupling to phonons increases the inversion, this corresponds to the behavior above the dashed line in Fig. 6(c).

The origin of this enhancement at large q can be understood by considering that for large q , the quantum dot state will come to thermal equilibrium with the phonon bath. Since the coupling to phonons depends on the prefactor $q(\Omega/\Lambda)^2$, the coupling to phonons will eventually switch off as $\Omega \rightarrow 0$. However, the larger the value of q , the later this switch off occurs, and so the longer system maintains thermal equilibrium with phonons. As the detuning Δ continues to increase at late times, the inversion of this equilibrated state therefore increases with increasing q .

IV. PHONON SPECTROSCOPY

A second application of the relative simplicity of Eq. (7) is to see how the phonon density of states can be recovered from spectroscopy using an appropriately designed pulse sequence. This would in principle allow direct experimental confirmation of the model phonon coupling $J(\omega) \propto \omega^3 \exp(-\omega^2/2\omega_c^2)$ as widely used^{8,14,16} in modeling quantum dots. In the following we present and compare two approaches to this, based on either short-time or long-time behavior, incorporating spontaneous decay in the long-time process.

A. Modified ARP protocol

The short-time approach uses a modified version of an ARP-like pulse sequence. We consider an ARP protocol divided into pieces, so that the sweep of $\Delta(t)$ is interrupted by a wait period T_w at a value Δ_w before completing the ARP sweep. The initial and final sweeps serve to map between initial or final eigenstates of s_z and eigenstates of r_z during the wait period. The final inversion depends on the effect of the phonons during the wait time, sampling the phonon density of states at a frequency $\Lambda_w = \sqrt{\Delta_w^2 + \Omega_w^2}$. During this wait time, Eq. (7) reduces to $\dot{p}_\downarrow = -\gamma_a p_\downarrow + \gamma_e p_\uparrow$, $\dot{p}_\uparrow = \gamma_a p_\uparrow - \gamma_e p_\downarrow$ in terms of the diagonal elements in the \mathbf{r} basis. The deviation from inversion of the final state after a given wait time T_w is thus given by:

$$\frac{1}{2} - s_z \simeq \frac{\gamma_{a,e}}{\gamma_a + \gamma_e} \left(1 - e^{-(\gamma_a + \gamma_e)T_w}\right), \quad (14)$$

where $\gamma_{a,e} = \gamma_{a,e}(\Omega_w, \Delta_w)$, and the numerator of the right hand side is γ_a for a forward sweep (Δ decreasing with time) and γ_e for a reverse sweep (Δ increasing with time). For long wait times, the excitations reach thermal equilibrium with the phonon bath, as expected¹⁸ and so s_z becomes independent of the phonon density of states.

For short wait times $(\gamma_a + \gamma_e)T_w \ll 1$, one finds $\frac{1}{2} - s_z \simeq \gamma_{a,e}(\Omega_w, 0)T_w$, thus by varying Ω_w one can directly map out the damping rate.

In order to extract the phonon density of states with some accuracy, the pulse sequence must be carefully chosen. At low temperatures, $\gamma_a \ll \gamma_e$, and so spectroscopy using the forward sweep is hard to achieve — the reduction in inversion is tiny for times T_w such that $T_w(\gamma_a + \gamma_e) \lesssim 1$ and tends to be dwarfed by effects of non-adiabaticity. Using a “reverse” ARP pulse produces a clearer signal. However, in order to have the signal dominated by the waiting time it is necessary for the wait time to be longer than the sweep, and the sweep to be sufficiently slow for all values of Ω_w . For this to be compatible with $T_w\gamma_e \lesssim 1$ it is helpful to choose $\Delta_w \neq 0$ so that the rate γ_e is suppressed by a factor $(\Omega_w/\Lambda_w)^2 < 1$. Combining these considerations, the pulse sequence:

$$\begin{aligned} \Delta(t) &= \Delta_w + \Delta_0 \left[\tanh\left(\frac{t+t_\Delta}{\tau_\Delta}\right) + \tanh\left(\frac{t-t_\Delta}{\tau_\Delta}\right) \right] \\ \Omega(t) &= -\frac{\Omega_w}{2} \left[\tanh\left(\frac{t+t_\Omega}{\tau_\Omega}\right) - \tanh\left(\frac{t-t_\Omega}{\tau_\Omega}\right) \right] \end{aligned} \quad (15)$$

gives the results shown in Fig. 7 with parameter values given in the figure caption.

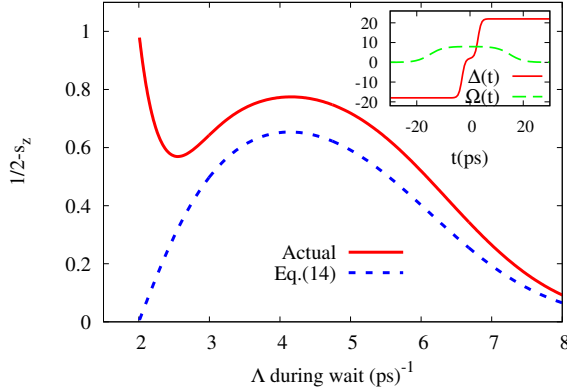


FIG. 7. (color online). Phonon spectroscopy using divided ARP pulse. Main figure, deviation from inversion following the protocol in Eq. (15) (solid), compared with the approximation of Eq. (14) (dashed line), plotted by varying Ω_w . Inset, time dependence of $\Delta(t)$ (solid) and $\Omega(t)$ (dashed), with parameters $\Delta_w = 2\text{ps}^{-1}$, $\Delta_0 = -10\text{ps}^{-1}$, $t_\Delta = T_w/2 = 3\text{ps}$, $\tau_\Delta = 1.2\text{ps}$, $t_\Omega = 15\text{ps}$, $\tau_\Omega = 5\text{ps}$, $T = 4\text{K}$.

There is a reasonable match between the prediction of Eq. (14) for decay during the wait time and the actual inversion, but the match is not perfect due to the effects of phonons during the initial and final sweep, as well as some remaining degree of non-adiabaticity (at small Ω_w). Nonetheless, one may invert Eq. (14) in order to extract the phonon density of states from the measured inversion, and the result of this procedure is shown as the dot-dashed line in the inset of Fig. 8. The reasonable agreement confirms that for such a pulse the final

inversion contains sufficient information to extract the phonon density-of-states; in practice one might include corrections to Eq. (14) by comparing an experiment directly to Eq. (7).

B. Steady state of driven open system

An alternate approach to reconstructing the phonon density of states arises by considering the long time behavior, allowing for both spontaneous decay as well as coupling to acoustic phonons, i.e.

$$\dot{\rho} \rightarrow \dot{\rho} - (\kappa/2)(s_+s_- \rho + \rho s_+s_- - 2s_- \rho s_+). \quad (16)$$

In particular, we consider the long time behavior under a constant driving, $\Omega(t) = \Omega_0$, $\Delta(t) = \Delta_0$. In this case, the long time behavior should be understood as a steady state arising from the balance of coupling to the phonon reservoir and the decay due to coupling to a photon reservoir. The pumping term Ω is necessary only in order to enable the phonon coupling to create and destroy excitations of the quantum dot. In the absence of spontaneous decay terms (no photon reservoir), the steady state would trivially be the thermal equilibrium of the system Hamiltonian, due to equilibration with the phonon reservoir. In this case, the phonon density of states does not appear, only the phonon temperature matters. However, the coupling to the photon reservoir drives the system into a non-thermal steady state, in which the balance of spontaneous decay rate and phonon coupling determines the state. One may then read out the phonon density of states from the steady state inversion achieved.

In the limit of small decays, i.e., $\kappa, \gamma_a, \gamma_e \ll \Omega, \Delta$, one may analytically solve the steady state equations for $s_{x,y,z}$ by expanding the steady state equations with respect to the decay rates (see appendix B for further details). One finds that at leading order:

$$s_z = \frac{-\Delta^2 \kappa + 2\Lambda \Delta (\gamma_a - \gamma_e)}{(\Omega^2 + 2\Delta^2) \kappa + 4\Lambda^2 (\gamma_a + \gamma_e)}. \quad (17)$$

As anticipated, this expression involves the ratio of phonon and spontaneous decay terms. In the limit $\kappa \rightarrow 0$, one recovers the thermal equilibrium result so that $s_z = (-\Delta/2\Lambda)(\gamma_e - \gamma_a)/(\gamma_a + \gamma_e)$, in which case the phonon density of states cancels, and no information about the phonon bath (other than temperature) appears in s_z . However for $\kappa \neq 0$, the steady state depends on the ratio of $\gamma^a/\kappa, \gamma^e/\kappa$, and this in turn allows the phonon density of states to be extracted from the final state.

Figure 8 shows how the phonon density of states can be reconstructed by extracting the steady state for a fixed value of Ω , and varying the pump detuning Δ . By inverting Eq. (17), and assuming the phonon temperature is known, one may extract the effective phonon density of states as shown in the inset. The density of states reconstructed this way matches the actual density of states used in the density matrix evolution very closely. It

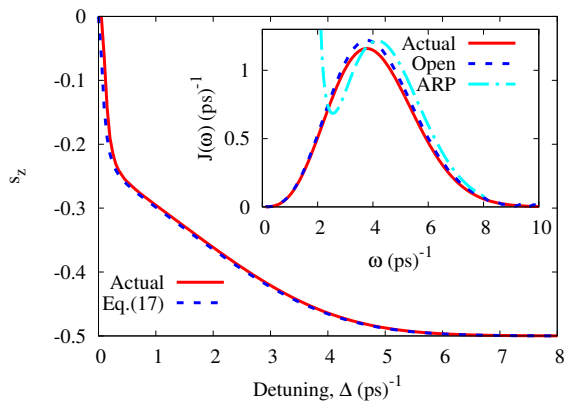


FIG. 8. (color online). Main figure: Steady state value of s_z with driving at $\Omega = 0.1(\text{ps})^{-1}$, with a spontaneous decay rate of $\kappa = 2(\text{ns})^{-1}$ as a function of the detuning, at $T = 20\text{K}$. Inset: comparison of actual phonon density of states $J(\omega)$ with the values reconstructed by inverting Eq. (17) and from the modified ARP approach, inverting Eq. (14) (parameters for modified ARP as in Fig. 7).

may also be possible to use recently developed variational approaches²⁷ to extend such phonon spectroscopy to more strongly coupled systems.

V. LINDBLAD VS NON-LINDBLAD APPROXIMATIONS

As mentioned above, the question of which Markovian approximation best corresponds to a given full density matrix equation was discussed extensively by Dumcke and Spohn²¹. The conclusion there is that in the limit of short bath correlation times, there exist multiple Markovian approximations which give have the same order of validity, as defined by the limiting behavior of $\|\rho^{\text{approx}} - \rho^{\text{full}}\|$ (where $\|\dots\|$ is the trace norm) as coupling to the bath vanishes. These different Markovian approximations are related by whether or not one averages over fast oscillating terms in the interaction picture. Without such averaging we reach Eq. (4), while averaging leads instead to Eq. (7). However, positivity of the density matrix is only preserved for the Lindblad form in Eq. (7), and so Dumcke and Spohn²¹ conclude that only this approach is correct.

It is often assumed that such a point is irrelevant as small decay rates (as are required for validity of the Markov approximation) imply that any possible violation of positivity is negligible. However, for problems involving weak decay and long time evolution, such as the current problem, positivity violation can occur for Eq. (4) even in regimes where the Markov approximation appears to be valid. This leads to unphysical results, as shown for example in Fig. 9. We note that for the Rabi oscillations studied by Ramsay *et al.*¹⁴ no positivity violation occurs for the parameters used and the results of

Eq. (4) and Eq. (7) are hardly distinguishable. Nonetheless, Eq. (7) is required to produce valid results across the problems considered in the current paper. Furthermore, as shown in the inset to Fig. 9, the Lindblad form continues to give qualitatively plausible results even at higher temperatures where Eq. (4) very strongly violates positivity.

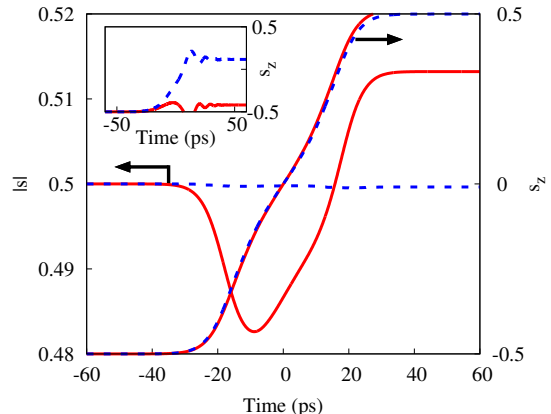


FIG. 9. (color online). Comparison of the dynamics obtained from the Lindblad [Eq. (7), dashed curves] and non-Lindblad [Eq. (4), solid curves] forms of time-dependent Markovian approximations, for the Gaussian ARP pulse, Eq. (11), with $\tau_0 = 2 \text{ ps}$, $T = 1 \text{ K}$, $a = 30 \text{ ps}^2$, $\Theta_0 = 5\pi$. For each approach both the magnitude of the pseudospin (Bloch) vector $|s|$ (left axis) and inversion s_z (right axis) are shown. At this low temperature, as discussed above, the Markov approximation holds reasonably well, yet the non-Lindblad form leads to unphysical results $|s|, |s_z| > 0.5$. The inset shows the inversion for a pulse with $a = 36 \text{ ps}^2$, $\Theta_0 = \pi$ at $T = 65 \text{ K}$; here the non-Lindblad form rapidly gives unphysical results $|s_z| > 0.5$, while the Lindblad form gives qualitatively reasonable dynamics.

There have been suggestions that time-dependent density-matrix equations which are not of the Lindblad form, such as those derived from the time-convolutionless (TCL) approach,¹² may in some cases ensure positivity.²⁸ However, Eq. (4) is essentially the result of the time-convolutionless approach at second order (TCL2). The only difference is that for TCL2, the lower limit on integrals over t' such as Eq. (6) is $t' = 0$, rather than $t' = -\infty$, corresponding to starting the system at $t = 0$ in a factorized state. Even for time independent Δ, Ω this means the coefficients in the density matrix evolution become time dependent, but eventually decay toward a steady state value. As such, for the ARP pulse, as long as the pulse duration is long compared to the bath correlation time, these additional time dependencies die out, and TCL2 becomes equivalent to the positivity-violating form in Eq. (4).

VI. CONCLUSIONS

In conclusion, we have shown how the Bloch-Redfield-Wangsness theory may be used to derive a time-dependent Lindblad form describing the dephasing of quantum-dot excitons by acoustic phonons in the presence of a driving laser field. We have outlined the application of this theory to recent ARP experiments^{4,5} on single quantum dots and predict, in agreement with numerical work,⁹ that phonons have a pronounced effect on ARP even at cryogenic temperatures. Their effect can, however, be almost eliminated by an appropriate choice of pulse shape. Furthermore, this pulse-shape dependence could allow forms of phonon spectroscopy based on ARP pulses or on off-resonant continuous-wave excitation. More generally, our approach captures the physics of dynamical, excitation-controlled dephasing, in which the driving field changes the eigenspectrum of the dot, and hence the decoherence and scattering rates. The resulting Lindblad form is straightforward to simulate, gives qualitatively reasonable results over wide parameter regimes, and is expected to be quantitatively accurate at low temperatures for slow pulses. It can be applied to a wide variety of pulse sequences, and the approach generalized to address a wide range of problems relating to the decoherence of solid-state qubits, such as the limitations on the creation of entangled states in coupled quantum dots,^{29–33} the persistence of entanglement in interacting solid-state systems, and the emission spectra of solid-state qubits in the strong-coupling regime.^{34,35}

ACKNOWLEDGMENTS

PRE acknowledges support from Science Foundation Ireland (09/SIRG/I1592). AOS acknowledges funding from the Carnegie Trust for the Universities of Scotland, and the St Andrews Undergraduate Research Internship Program. JK acknowledges useful discussions with B. Lovett, F. B. F. Nissen, P. Öhberg, and support from EPSRC (EP/G004714/2 and EP/I031014/1).

Appendix A: Derivation of secularized density matrix equation

This appendix provides further details of the derivation of the time-dependent Markovian Lindblad form in Eq. (7). Following the usual approach,¹² working in the interaction picture, the effects of the system-bath coupling on the system density matrix can be included to second order by writing:

$$\dot{\tilde{\rho}} = - \int_{-\infty}^t dt' \text{Tr}_B \left[\tilde{H}_c(t), \left[\tilde{H}_c(t'), \tilde{\rho}(t') \otimes \tilde{\rho}_B(0) \right] \right] \quad (\text{A1})$$

where tilde indicates the interaction picture, $\tilde{\rho}_B$ is the phonon bath matrix, and H_c is given in Eq. (2).

In the case that Δ, Ω vary slowly with time, we may effectively transform the coupling Hamiltonian to the interaction picture by using the instantaneous eigenstates (dressed states) giving

$$H_c(t) = P(t)\Phi(t) = e^{itH_{\text{dot}}} s_z e^{-itH_{\text{dot}}} \sum_q (g_q b_q e^{-i\nu_q t} + g_q^* b_q^\dagger e^{i\nu_q t}), \quad (\text{A2})$$

where ν_q is the phonon frequency. We transform to the instantaneous dressed states, defining spin operators $\mathbf{r} = R\mathbf{s}$, with R a rotation by angle $\tan^{-1} \Omega/\Delta$ around the y -axis. Then the coupling operators become

$$P(t) = \frac{\Delta}{\Lambda} r_z + \frac{\Omega}{2\Lambda} (r_+ e^{i\Lambda t} + r_- e^{-i\Lambda t}), \quad (\text{A3})$$

where $\Lambda = \sqrt{\Omega^2 + \Delta^2}$ is the splitting of the instantaneous eigenstates, and r_\pm cause transitions between these states.

Note that for a time-dependent Hamiltonian, the true interaction-picture form is obtained with a unitary transformation involving a time-ordered exponential, $U = T e^{-i \int^t H_{\text{dot}}(t') dt'}$, and this operator is not generally approximated by the form in Eq. (A2). However, in the following we use the form in Eq. (A2) only to calculate the effects of phonons on short timescales, $t_c \sim 1/\omega_c$, with the final equation for the density matrix obtained by undoing this formal transformation. Thus we expect that the Hamiltonian part of the dynamics is not approximated in the result, while the dissipative part is correct provided $t_c d\Delta/dt, t_c d\Omega/dt \ll \Lambda$. These conditions are well satisfied for the protocols considered in this paper.

With these forms of $P(t), \Phi(t)$, we may then follow the normal steps of tracing over the phonon bath to give the system density matrix equation:

$$\begin{aligned} \dot{\tilde{\rho}} = - \int d\nu J(\nu) \int dt' \Big\{ & [P(t)P(t')\tilde{\rho}(t') - P(t')\tilde{\rho}(t')P(t)] \\ & \times \left[(n_\nu + 1)e^{-i\nu(t-t')} + n_\nu e^{i\nu(t-t')} \right] \\ & - [P(t)\tilde{\rho}(t')P(t') - \tilde{\rho}(t')P(t')P(t)] \\ & \times \left[(n_\nu + 1)e^{i\nu(t-t')} + n_\nu e^{-i\nu(t-t')} \right] \Big\}, \end{aligned} \quad (\text{A4})$$

where n_ν is the thermal occupation of the phonons at frequency ν . After performing the integrals over frequency the remaining integral contains factors which are sharply peaked functions of $t - t'$, decaying over a timescale $1/\omega_c$. $\rho(t')$ and $\Delta(t'), \Omega(t')$ vary little over this timescale, and so may be approximated by their values at t . However, $P(t')$ may vary over this timescale due to the time-dependence arising from the transformation to the interaction picture. If we approximate $\tilde{\rho}(t') \simeq \tilde{\rho}(t)$ and perform no other steps, this leads to Eq. (4), which as noted before, is not of Lindblad form.

Following Dumcke and Spohn²¹, the corresponding Lindblad form arises by “secularizing” Eq. (A4). This

corresponds to averaging the above equation over a time short compared to decay rates, but long compared to the timescales of the system Hamiltonian — the fact that such a timescale exists is implicit in the use of a perturbative (Born) approximation. We start from Eq. (4), with $P(t)$ as defined in Eq. (5), and writing $Q(t)$ in the generic form:

$$Q(t) = \Gamma_z r_z + \Gamma_+ r_+ e^{i\Lambda t} + \Gamma_- r_- e^{-i\Lambda t}. \quad (\text{A5})$$

This follows directly from performing the integrals in Eq. (6), and so Γ_z, Γ_\pm are various frequency integrals over $J(\nu)$. Multiplying $P(t), Q(t)$ and integrating over a time long compared to $1/\Lambda$, only those terms with equal and opposite t dependence will survive, i.e. those terms involving $r_z r_z, r_+ r_-$ or $r_- r_+$. The secularized Eq. (4)

thus becomes:

$$\begin{aligned} \dot{\rho} = & \frac{\Delta}{\Lambda} (\Gamma_z + \Gamma_z^*) (r_z \tilde{\rho} r_z - \tilde{\rho}) \\ & - \frac{\Omega}{2\Lambda} [\Gamma_+ (r_- r_+ \tilde{\rho} - r_+ \tilde{\rho} r_-) + \Gamma_+^* (\tilde{\rho} r_- r_+ - r_+ \tilde{\rho} r_-)] \\ & - \frac{\Omega}{2\Lambda} [\Gamma_- (r_+ r_- \tilde{\rho} - r_- \tilde{\rho} r_+) + \Gamma_-^* (\tilde{\rho} r_+ r_- - r_- \tilde{\rho} r_+)]. \end{aligned}$$

The vanishing of the phonon density of states as $\omega \rightarrow 0$ ensures that $\Gamma_z + \Gamma_z^* = 0$, and the remaining terms take the form of the Lindblad decay and phonon Lamb shift terms as given in Eq. (7).

Appendix B: Steady state of driven open system for small decay rates

This appendix gives further details of the derivation of Eq. (17), the steady state s_z found for the driven system in the presence of both phonon induced dephasing and spontaneous decay (photon emission). Including spontaneous decay as in Eq. (16) in addition to the density matrix evolution given in Eq. (7) one may write equations of motion for the Bloch vector $s_{x,y,z}$ of the form:

$$\dot{s}_x = -\frac{\Omega}{\Lambda}(\gamma_a - \gamma_e) - \left[\frac{\kappa}{2} + \frac{\Delta^2 + 2\Omega^2}{\Lambda^2}(\gamma_a + \gamma_e) \right] s_x - \Delta s_y + \frac{\Delta\Omega}{\Lambda^2}(\gamma_a + \gamma_e)s_z \quad (\text{B1})$$

$$\dot{s}_y = \Delta s_x - (\kappa/2 + \gamma_a + \gamma_e)s_y + \Omega s_z \quad (\text{B2})$$

$$\dot{s}_z = -\frac{\kappa}{2} + \frac{\Delta}{\Lambda}(\gamma_a - \gamma_e) + \frac{\Delta\Omega}{\Lambda^2}(\gamma_a + \gamma_e)s_x - \Omega s_y - \left[\kappa + \frac{2\Delta^2 + \Omega^2}{\Lambda^2}(\gamma_a + \gamma_e) \right] s_z. \quad (\text{B3})$$

In the limit of vanishing decay terms $\kappa, \gamma_a, \gamma_e \rightarrow 0$, it is clear that the steady state requires $\Delta s_x + \Omega s_z = 0, s_y = 0$. At leading order in the decay terms, one finds $s_y \sim \mathcal{O}(\kappa, \gamma_a, \gamma_e)$, and so one may continue to use

$s_x = -(\Omega/\Delta)s_z$ as the solution of $\dot{s}_y = 0$ up to order $\mathcal{O}(\kappa^2, \gamma_a^2, \gamma_e^2)$. Using this, the remaining two equations $\dot{s}_{x,z} = 0$ can be solved by eliminating s_y , to give Eq. (17).

¹ A. N. Vamivakas and M. Atatüre, Contemp. Phys. **51**, 17 (2010).

² T. H. Stievater, X. Li, D. G. Steel, D. Gammon, D. S. Katzer, D. Park, C. Piermarocchi, and L. J. Sham, Phys. Rev. Lett. **87**, 133603 (2001).

³ A. J. Ramsay, Semicond. Sci. Technol. **25**, 103001 (2010).

⁴ Y. Wu, I. M. Piper, M. Ediger, P. Brereton, E. R. Schmidgall, P. R. Eastham, M. Hugues, M. Hopkinson, and R. T. Phillips, Phys. Rev. Lett. **106**, 067401 (2011).

⁵ C.-M. Simon, T. Belhadj, B. Chatel, T. Amand, P. Renucci, A. Lemaitre, O. Krebs, P. A. Dalgarno, R. J. Warburton, X. Marie, and B. Urbaszek, Phys. Rev. Lett. **106**, 166801 (2011).

⁶ E. R. Schmidgall, P. R. Eastham, and R. T. Phillips, Phys. Rev. B **81**, 195306 (2010).

⁷ P. R. Eastham and R. T. Phillips, Phys. Rev. B **79**, 165303 (2009).

⁸ A. J. Ramsay, A. V. Gopal, E. M. Gauger, A. Nazir, B. W. Lovett, A. M. Fox, and M. S. Skolnick, Phys. Rev. Lett. **104**, 017402 (2010).

⁹ S. Lüker, K. Gawarecki, D. E. Reiter, A. Grodecka-Grad, V. M. Axt, P. Machnikowski, and T. Kuhn, Phys. Rev. B **85**, 121302 (2012).

¹⁰ D. E. Reiter, S. Lüker, K. Gawarecki, A. Grodecka-Grad, P. Machnikowski, V. M. Axt, and T. Kuhn, arXiv:1207.6660.

¹¹ K. Schuh, F. Jahnke, and M. Lorke, Appl. Phys. Lett. **99**, 011105 (2011).

¹² H.-P. Breuer and F. Petruccione, *The Theory of Open Quantum Systems* (Oxford University Press, Oxford,

- 2007).
- ¹³ A. Vagov, M. D. Croitoru, V. M. Axt, T. Kuhn, and F. M. Peeters, *Phys. Rev. Lett.* **98**, 227403 (2007).
 - ¹⁴ A. Ramsay, T. M. Godden, S. J. Boyle, E. M. Gauger, A. Nazir, B. W. Lovett, A. M. Fox, and M. S. Skolnick, *Phys. Rev. Lett.* **105**, 177402 (2010).
 - ¹⁵ D. P. S. McCutcheon and A. Nazir, *New J. Phys.* **12**, 113042 (2010).
 - ¹⁶ A. J. Ramsay, T. M. Godden, S. J. Boyle, E. M. Gauger, A. Nazir, B. W. Lovett, A. V. Gopal, A. M. Fox, and M. S. Skolnick, *J. Appl. Phys.* **109**, 102415 (2011).
 - ¹⁷ A. Nazir, *Phys. Rev. B* **78**, 153309 (2008).
 - ¹⁸ J. D. Cresser, *J. Mod. Opt.* **39**, 2187 (1992).
 - ¹⁹ R. K. Wangsness and F. Bloch, *Phys. Rev.* **89**, 728 (1953).
 - ²⁰ A. G. Redfield, *Phys. Rev.* **98**, 1787 (1955).
 - ²¹ R. Dumcke and H. Spohn, *Z. Phys. B* **34**, 419 (1979).
 - ²² H. Spohn, *Rev. Mod. Phys.* **52**, 569 (1980).
 - ²³ T. M. Stace, A. C. Doherty, and S. D. Barrett, *Phys. Rev. Lett.* **95**, 106801 (2005).
 - ²⁴ E. M. Gauger, S. C. Benjamin, A. Nazir, and B. W. Lovett, *Phys. Rev. B* **77**, 115322 (2008).
 - ²⁵ V. S. Malinovsky and J. L. Krause, *Eur. Phys. J. D* **14**, 147 (2001).
 - ²⁶ S. Guérin, S. Thomas, and H. R. Jauslin, *Phys. Rev. A* **65**, 023409 (2002).
 - ²⁷ D. McCutcheon, N. Dattani, E. Gauger, B. Lovett, and A. Nazir, *Phys. Rev. B* **84**, 081305 (2011).
 - ²⁸ R. S. Whitney, *J. Phys. A: Math. Theor.* **41**, 175304 (2008).
 - ²⁹ C. Creatore, R. T. Brierley, R. T. Phillips, P. B. Littlewood, and P. R. Eastham, *arXiv:1112.5964*.
 - ³⁰ R. G. Unanyan, N. V. Vitanov, and K. Bergmann, *Phys. Rev. Lett.* **87**, 137902 (2001).
 - ³¹ Z. Kis and E. Paspalakis, *J. Appl. Phys.* **96**, 3435 (2004).
 - ³² U. Hohenester, J. Fabian, and F. Troiani, *Optics Commun.* **264**, 426 (2006).
 - ³³ S. K. Saikin, C. Emary, D. G. Steel, and L. J. Sham, *Phys. Rev. B* **78**, 235314 (2008).
 - ³⁴ Y. Makhlin, G. Schön, and A. Shnirman, *Rev. Mod. Phys.* **73**, 357 (2001).
 - ³⁵ P. Kaer, T. R. Nielsen, P. Lodahl, A.-P. Jauho, and J. Mørk, *Phys. Rev. Lett.* **104**, 157401 (2010).